A novel ferroptosis-related gene signature for overall survival prediction and immune infiltration in patients with breast cancer

YAN ZHANG[1,2], YIRAN LIANG[1], YAJIE WANG[1], FANGZHOU YE[1], XIAOLI KONG[1] and QIFENG YANG[1,3,4]

[1]Department of Breast Surgery, Qilu Hospital, Cheeloo College of Medicine, Shandong University, Jinan, Shandong 250012; [2]Department of Breast Surgery, Jinan Central Hospital, Cheeloo College of Medicine, Shandong University, Jinan, Shandong 250013; [3]Pathology Tissue Bank, Qilu Hospital of Shandong University; [4]Research Institute of Breast Cancer, Shandong University, Jinan, Shandong 250012, P.R. China

Received May 8, 2022; Accepted August 3, 2022

DOI: 10.3892/ijo.2022.5438

Abstract. Breast cancer is the most prevalent type of cancer among women worldwide. The heterogeneous nature of breast cancer poses a serious challenge for prognostic prediction and individualized therapies. Recently, ferroptosis, an iron-dependent form of programmed cell death, has been reported to serve a significant role in the regulation of the biological behavior of tumors. Several studies have revealed the prognostic significance of the ferroptosis-related gene (FRG) model; however, additional efforts are required to elucidate the details. Moreover, genes that modulate ferroptosis may be promising candidate bioindicators in cancer therapy. The present study systematically assessed the expression profiles of FRGs to reveal the relationship between FRGs and the prognostic features of patients with breast cancer based on data obtained from the Gene Expression Omnibus and Molecular Taxonomy of Breast Cancer International Consortium. Using a non-negative matrix factorization clustering method, patients with breast cancer were classified into two sub-groups (cluster 1 and cluster 2) based on the expression of FRGs. Furthermore, Cox regression, and least absolute shrinkage and selection operator methods were used to construct a risk score formula comprised of nine genes, which stratified patients with breast cancer into two risk groups. Patients belonging to the high-risk group exhibited significantly shorter overall survival (OS) time compared with patients in the low-risk group. The prognostic value of this signature was further verified in the training and validation cohorts. The results for univariate and multivariate Cox regression analyses indicated that risk score acted as an independent predictor for OS. Subsequently, a nomogram was constructed. Receiver operating characteristic analysis further confirmed that the resulting nomogram exhibited powerful discriminatory ability. Functional analysis revealed that the immune environment differed notably between the two groups and indicated an association between ferroptosis and breast cancer proliferation, migration and drug resistance. Taken together, the present study demonstrated that FRGs were significantly associated with breast cancer progression, and thus could be used as novel biomarkers for prognostic prediction and individualized treatment of patients with breast cancer.

Correspondence to: Professor Qifeng Yang, Department of Breast Surgery, Qilu Hospital, Cheeloo College of Medicine, Shandong University, 107 Wenhua Xi Road, Jinan, Shandong 250012, P.R. China
E-mail: qifengy_sdu@163.com

Key words: breast cancer, ferroptosis, gene signature, prognosis, immune microenvironment

Introduction

In previous years, a gradual increase has been detected in the annual incidence of breast cancer worldwide. Notably, breast cancer can be divided into several subtypes according to the presence of receptors on the cell surface (1). In 2018, there were >2,000,000 new cases of breast cancer and >620,000 deaths associated with breast cancer worldwide (2). Previous studies have reported that 20-30% of patients with breast cancer are diagnosed with distant metastases at the time of primary diagnosis, and 25% of primary non-metastatic cases eventually result in metastases. Despite development being made in diagnostic and therapeutic methods, the prognosis of patients with breast cancer remains unsatisfactory, particularly concerning metastatic breast cancer (3). Moreover, the issues of drug resistance and heterogeneity in breast cancer are often attributed to treatment failure and tumor recurrence (4). In previous studies, several markers have been used for the diagnostic and prognostic prediction of breast cancer. For example, phosphorylated-STAT3 expression has been reported to be associated with the survival and mammographic density of patients with breast cancer (5). In addition, ceruloplasmin has been shown to be correlated with immune infiltration and may serve as a prognostic biomarker in breast cancer (6). However, a single biomarker does not show better predictive performance compared with previously existing predictive models, thus it is urgent to explore new multi-gene models to improve diagnostic and prognostic predictions in patients with breast cancer. Furthermore, identification of novel and effective therapeutic targets and predictive models using biomarkers

may contribute to the comprehensive elucidation of the potential mechanisms involved in the development and progression of breast cancer, which would further aid in improving the overall survival (OS) rate in patients with breast cancer.

It has previously been reported that various cancer treatment methods can induce cell-specific programmed cell death, which is known to be closely associated with tumor development and progression (7). Ferroptosis, a novel form of programmed cell death first identified in 2012 (8), has gained increasing attention as a potential therapeutic pathway for cancer treatment. Ferroptosis is characterized by iron-dependent lipid peroxide accumulation, which differs from traditional apoptosis, autophagy or necrosis in terms of morphology, biochemistry and genetics (8). Numerous genes have previously been identified as markers, inducers or inhibitors of ferroptosis (9-11), collectively called ferroptosis-related genes (FRGs), such as GPX4, CISD1 and NRF2. Previous studies have identified a pivotal role of ferroptosis in tumor progression and therapeutics (12-14). Although the sensitivity of different types of tumor cells towards ferroptosis are diverse, a combination of erastin (an inducer of ferroptosis) and chemotherapeutics could improve curative effects in various types of cancer, such as ovarian cancer (15), lung cancer (16) and breast cancer (17). Moreover, ferroptosis has been reported to be associated with the prognosis of various types of cancer, and ferroptosis-related prognostic models have been constructed in glioma (18), melanoma (19) and renal cell carcinoma (20), further indicating the potential value of FRGs as prognostic markers and therapeutic targets in human cancer. Several reports have shown that ferroptosis is strongly associated with breast cancer (21,22), indicating that ferroptosis may be considered an important biomarker in breast cancer. However, single genes alone cannot comprehensively predict the diagnosis and survival of patients with breast cancer. Hence, additional efforts are required to establish ferroptosis-related predictive models for prediction and treatment of breast cancer to further improve the prognosis of patients with breast cancer.

The tumor immune microenvironment is typically comprised of immune cells and immune-related molecules that are present around the tumor (23,24), highlighting the significant role of the immune system in tumor-stroma interactions and the response towards immunotherapy. In recent years, the association between immune cells and immune molecules with iron metabolism has gained considerable attention (25). Various types of immune cells, including Th1 cells, natural killer (NK) T cells and macrophages, have previously been shown to be associated with the maintenance of iron homeostasis (26). Notably, ferroptosis in tumor cells can increase the expression of tumor antigens that bind immune cells, which further promotes the antitumor efficacy of immunotherapy (27). However, the role of ferroptosis in immunotherapy of breast cancer has not been fully elucidated.

In the present study, a ferroptosis-related prognostic model was constructed based on mRNA expression profiles and clinical data of patients with breast cancer obtained from the Gene Expression Omnibus GSE20685 cohort (28). The model was further validated using data from the Molecular Taxonomy of Breast Cancer International Consortium (METABRIC) cohort (29). Moreover, gene signature characteristics in the tumor microenvironment were evaluated using single-sample gene set enrichment analysis (ssGSEA) and immune infiltration analysis. The results of the present study may provide novel therapeutic targets for the management of breast cancer. Additionally, the present study may assist in improving clinical outcomes of patients with breast cancer when subjected to personalized treatment.

Materials and methods

Data collection. The expression profiling of FRGs and the corresponding clinical information of 327 patients with breast cancer, including their age, TNM stage and survival information, were obtained from the GSE20685 database (https://www.ncbi.nlm.nih.gov/geo/) and used as the training cohort. Moreover, the gene expression and clinical information of 1,904 patients with breast cancer from the METABRIC database were downloaded from cBioPortal (https://www.cbioportal.org/) as previously reported (30), which was used as the validation cohort. FRGs were identified from the GeneCards database (https://www.genecards.org/), FerrDb database (http://www.zhounan.org/ferrdb/) and other related literature (31,32). Consequently, a total of 314 FRGs were included in the analysis.

Identification of breast cancer subclasses. A filtering procedure was first conducted according to a previous study (31). The low median absolute deviation (MAD) value, a robust statistic to measure the statistical deviation, was calculated for each candidate gene. The genes with a MAD value <0.5 were excluded. Subsequently, R software was used for further analysis (33), and the R packages were downloaded from the R website (https://cran.r-project.org/mirrors.html). The non-negative matrix factorization (NMF) clustering method was applied using the 'NMF' R package (34) with the default parameters 'nrun=10' and 'seed=1'. The best cluster number was selected as the coexistence correlation coefficient k=2 (35). T-distributed stochastic neighbor embedding (t-SNE) analysis was then performed to validate the distribution of different groups using the 'Rtsne' R package (https://github.com/jkrijthe/Rtsne). The related parameters were: dims=2, perplexity=10, verbose=F, max_iter=500, check_duplicates=F. Moreover, principal components analysis (PCA) was performed to assess the differences in expression between the subtypes.

Establishment and validation of the prognostic predictive signature. Univariate Cox regression analysis was first performed to screen the genes related to OS in patients with breast cancer using the 'survival' package in R software (https://github.com/therneau/survival). Genes that were P<0.05 were considered statistically significant and were incorporated into the subsequent least absolute shrinkage and selection operator (LASSO) Cox regression using the 'Glmnet' package in R software (36). The related parameters were: lasso family='cox', maxit=1000, nfold=10, α=1. Subsequently, based on the multivariate Cox regression analysis for these genes, a prognostic signature was constructed. The prognostic risk score was calculated based on the regression coefficients (β) in the multivariate Cox regression model and the expression levels of the genes. The risk score calculation was as follows: Risk score=(-0.854 x expression of YWHAE)+(-0.852 x expression of

CD44)+(-0.683xexpressionofHILPDA)+(-0.284xexpressionof IFNG) + (-0.272 x expression of MYB) + (0.511 x expression of DBN1) + (0.554 x expression of HES1) + (0.652 x expression of HSPB1) + (1.107 x expression of SLC11A2). Receiver operating characteristic (ROC) analysis was performed to determine the optimal cut-off value, in order to divide the patients with breast cancer into the high- and low-risk groups. Kaplan-Meier (K-M) survival analysis followed by log-rank test were performed to evaluate the prognosis between two groups in both the training cohort and validation cohort. Moreover, the time-dependent ROC curves were used to validate the sensitivity and accuracy of the prognostic signature on OS in two cohorts.

Establishment of the nomogram model. Univariate Cox regression analysis was performed to evaluate the prognostic values of the clinical information (i.e., age, grade and TNM stage) and risk score. Subsequently, multivariate Cox regression analysis was applied to determine the independent prognostic factors to predict the survival of patients with breast cancer. By combining the TNM stage and risk score, a nomogram was constructed using the survival rate and the 'RMS' R package (https://github.com/harrelfe/rms). The related parameters were: cmethod='KM', method='boot', u=time, B=1000. According to the nomogram, the total point of each patient was calculated. The calibration curve was employed to evaluate the consistency between the actual and predicted survival rates. ROC curve analysis was applied to validate the sensitivity and specificity of the nomogram compared to that of a single independent predictor for predicting OS. Decision curve analysis (DCA) was performed using the 'RMDA' package (http://mdbrown.github.io/rmda/) with the parameters 'family=binomial(link='logit')' to evaluate the clinical predictive effect obtained by the nomogram compared to a single independent prognostic predictor.

Estimation of immune infiltration. The estimation of stromal and immune cells in malignant tumor tissues using expression data (ESTIMATE) algorithm was applied to the GSE20685 and METABRIC cohorts to calculate the immune score, stromal score and tumor purity, which reflected the enrichment of immune and stromal cell gene signatures (37). The CIBERSORT analysis was performed in two cohorts to assess the infiltration levels of 22 human immune cell subpopulations using the 'CIBERSORT' R package with the parameters 'perm=100' and 'QN=TRUE' (38). Subsequently, the fractions of 16 immune cells and the scores of 13 immune-related functions in two cohorts were respectively calculated using the ssGSEA with the 'GSVA' R package (39). The related parameters were: method='ssgsea', kcdf='Gaussian', abs.ranking=TRUE. To predict whether each subgroup could benefit from immunotherapy, the similarity of the gene expression profiles was calculated between the subgroups and the previously published data from patients with melanoma treated with immunotherapy based on the SubMap analysis (40).

Prediction of potential drugs based on drug-gene correlation analyses. The drug z-scores and the corresponding gene expression of the NCI-60 cancerous cell lines were downloaded from the CellMiner database (https://discover.nci.nih.gov/cellminer/loadDownload.do) (41). A higher z-score is indicative of higher sensitivity to the corresponding drug. Subsequently, the Pearson correlation between gene expression and drug sensitivity was analyzed. To perform this, the 'impute' (https://bioconductor.org/packages/impute/) and 'limma' R packages (42) were used for data processing, and the 'ggplot2' (https://ggplot2.tidyverse.org) and 'ggpubr' (https://rpkgs.datanovia.com/ggpubr/) R packages were used for visualization. The drug information was obtained from the DrugBank database (https://www.drugbank.ca/).

Cell culture. The human breast cancer cell lines MDA-MB-231 (HTB-26), MDA-MB-468 (HTB-132), MCF-7 (HTB-22) and T47D (HTB-133) were obtained from the American Type Culture Collection. The cells were cultured in DMEM (Macgene Biotechnology) supplemented with 10% FBS (Gibco; Thermo Fisher Scientific, Inc.) and 1% penicillin-streptomycin (Macgene Biotechnology) in a standard humidified incubator supplied with 5% CO_2 at 37˚C.

MTT assay. Erastin (10 or 20 μM; cat. no. HY-15763) and ferrostatin-1 (Fer-1; 10 μM; cat. no. HY-100579) were purchased from MedChemExpress. A total of $3x10^3$ cells were plated into 96-well plates and incubated overnight. After treating the breast cancer cells (MDA-MB-231, MDA-MB-468, MCF-7 and T47D) with the reagents erastin, ferrostatin-1, paclitaxel (MedChemExpress), doxorubicin (MedChemExpress) or tamoxifen (MilliporeSigma) at the indicated concentrations for 48 h at 37˚C, 20 μl 5 mg/ml MTT was added to each well, and the cells were further incubated for 4 h at 37˚C, after which 200 μl DMSO was added. The absorbance was measured at 490 nm using a microplate reader (Bio-Rad Laboratories, Inc.).

Migration assay. A Transwell system (24 wells; pore size, 8 μm; a polycarbonate membrane) was used for the *in vitro* migration assays. The breast cancer cells (MDA-MB-231, MDA-MB-468, MCF-7 and T47D) were pretreated with 10 μM erastin with or without 10 μM ferrostatin-1 for 24 h at 37˚C. DMSO was used as vehicle. Subsequently, $1x10^5$ cells were suspended in 200 μl serum-free medium and added to the upper chamber, and 700 μl medium supplemented with 20% FBS was added to the lower chamber. Cells were incubated for 24-48 h, after which the cells that had attached to the lower surface were fixed with methanol for 15 min and stained with 0.2% crystal violet for 20 min at room temperature. Finally, the migrated cells were imaged using a light microscope (Olympus Corporation) and quantified.

Reactive oxygen species (ROS) analysis. A reactive oxygen species assay kit (cat. no. S0033S; Beyotime Institute of Biotechnology) was used to detect cellular ROS levels. MDA-MB-231 and MDA-MB-468 cells were plated in a 6-well plate. When cell density reached 80%, the cells were treated with 10 or 20 μM erastin or 10 μM ferrostatin-1 for 24 h at 37˚C. The treated cells were collected and washed three times with PBS. Serum-free DMEM supplemented with 2 μM DCFH-DA (1:5,000; Beyotime Institute of Biotechnology) was added to the cells and incubated at 37˚C for 30 min. After incubation, the cells were washed and resuspended in 300 μl

PBS, and ROS accumulation in 10,000 cells was detected using a flow cytometer (BD Accuri™ C6 Plus Flow Cytometer) and BD Accuri C6 Plus software (BD Biosciences) with an excitation wavelength of 488 nm and an emission wavelength of 525 nm. Analysis was performed using FlowJo version 10.6.2 (FlowJo LLC).

Statistical analysis. Statistical analyses were performed using R, SPSS version 19.0 (IBM Corp), and GraphPad Prism version 8 (GraphPad Software, Inc.). Data from at least three independent experiments are presented as the mean ± standard deviation. χ^2 test was used to evaluate the differences in clinicopathological features between the two clusters of patients with breast cancer. K-M survival analysis and the log-rank test were performed to evaluate differences in the OS between the two groups. Univariate, LASSO and multivariate Cox regression analyses were performed to identify the independent prognostic factors. ROC curve analysis was performed to assess the sensitivity and specificity of the prognostic model. Unpaired Student's t-test was used to analyze the differences between unpaired breast cancer tissues and normal tissues in the databases. Comparisons in datasets containing multiple groups were analyzed using a one-way ANOVA followed by a post-hoc Dunnett's test. Pearson correlation analysis was used to evaluate the correlation between gene expression and drug sensitivity. $P<0.05$ was considered to indicate a statistically significant difference.

Results

Classification of patients with breast cancer based on FRGs. A flow chart of the study procedure is shown in Fig. 1A. Following filtration using MAD, a total of 171 genes were subjected to NMF analysis to identify different groups of patients with breast cancer. To identify the optimal k-value, cophenetic correlation coefficients were calculated. For k=2, the consensus matrix heatmap maintained a clear and sharp boundary, indicating that the samples exhibited stable and robust clusters (Figs. 1B and S1). Consequently, the patients with breast cancer were divided into two clusters, designated as cluster 1 and cluster 2. In particular, 187 and 140 samples were included in cluster 1 (C1) and cluster 2 (C2), respectively. The results of t-SNE analysis evidently confirmed that these two clusters were largely in concordance with two-dimensional coordinate systems (Fig. 1C). PCA analysis also indicated that patients with breast cancer belonging to different clusters were distributed in two directions (Fig. 1D). Furthermore, survival analysis demonstrated that patients with breast cancer in cluster 2 exhibited a shorter survival time compared with patients in cluster 1 (Fig. 1E). The study further analyzed the association between expression of FRGs and the clinical status of each patient in the two clusters (Fig. 1F; Table SI). The results indicated significant differences in the ferroptosis-related molecular features between the two patient clusters. Clinical characteristics of these two clusters are presented in Table SII. A χ^2 test revealed that there were more patients with an advanced TNM stage in cluster 2, suggesting that the expression of FRGs was closely associated with tumor progression of patients with breast cancer.

Identification of prognostic FRGs in breast cancer. The study further evaluated the prognostic role of FRGs in breast cancer. In the training cohort, 62 genes were identified to be associated with OS, using univariate Cox regression analysis ($P<0.05$; Table SIII). Furthermore, 37 genes were considered to be associated with the prognosis of breast cancer, based on the results of LASSO regression analysis (Fig. 2A). Multivariate Cox regression analysis was further performed, and nine genes were finally selected for the construction of a prognostic model on the basis of expression levels and regression coefficients (Fig. 2B and C; Table I). The risk scores for each patient were calculated, and the patients were classified into low-risk and high-risk groups based on the optimal cut-off value. The results revealed that high-risk patients had a significantly shorter OS and higher mortality rates compared with the low-risk patients with breast cancer (Fig. 3A and B). Notably, the area under the curve (AUC) values were recorded to be 0.670, 0.705 and 0.742 in the time-dependent ROC at 3, 5 and 10 years, respectively (Fig. 3C), which indicated significant specificity and sensitivity of the prognostic signature in the prediction of OS. The METABRIC database was further used as an external validation cohort to validate the predictive efficiency of the developed prognostic model. To clarify the classification of the patients with breast cancer into high-risk and low-risk groups, risk scores for the patients from METABRIC were calculated, using the aforementioned formula. In concordance with previous results, patients with breast cancer in the high-risk group exhibited a significantly lower OS and higher mortality rate compared with the patients in the low-risk group (Fig. 3D and E). Moreover, AUC values of 0.573, 0.578 and 0.574 were recorded for the 3-, 5- and 10-year OS, respectively (Fig. 3F).

Construction and validation of a predictive nomogram for patients with breast cancer. Univariate and multivariate Cox regression analyses were performed to evaluate whether the prognostic value of the nine gene model in the prediction of OS was independent of other traditional clinicopathological parameters. The results of the analysis indicated that the TNM stage and risk score of the prognostic signature acted as independent predictors of OS (Fig. 4A). C-index was recorded to be 0.75. To quantify prediction results for individual survival probability at 3, 5 and 10 years, a survival nomogram prediction model was constructed (Fig. 4B). The calibration curves showed an optimal agreement consistency between observed and predicted OS rates at 3, 5 and 10 years (Fig. 4C). Moreover, AUCs were recorded to be 0.778, 0.775 and 0.794 with the nomogram for 3-, 5- and 10-year OS, respectively. The model was considered to be superior to a single independent predictive factor (Fig. 4D), which demonstrated the superior predictive value of the nomogram. To further evaluate the importance of the nomogram in clinical decision-making, DCA was performed. DCA is a novel reliable evaluation tool that is used to quantify the clinical value of a nomogram (43). The results of DCA indicated that the nomogram provided optimal clinical decision-making benefits at 3, 5 and 10 years compared with a single independent predictive factor (Fig. 4E). Additionally, these results indicated that the nine-FRG prognostic model served as a reliable prognostic indicator for patients with breast cancer.

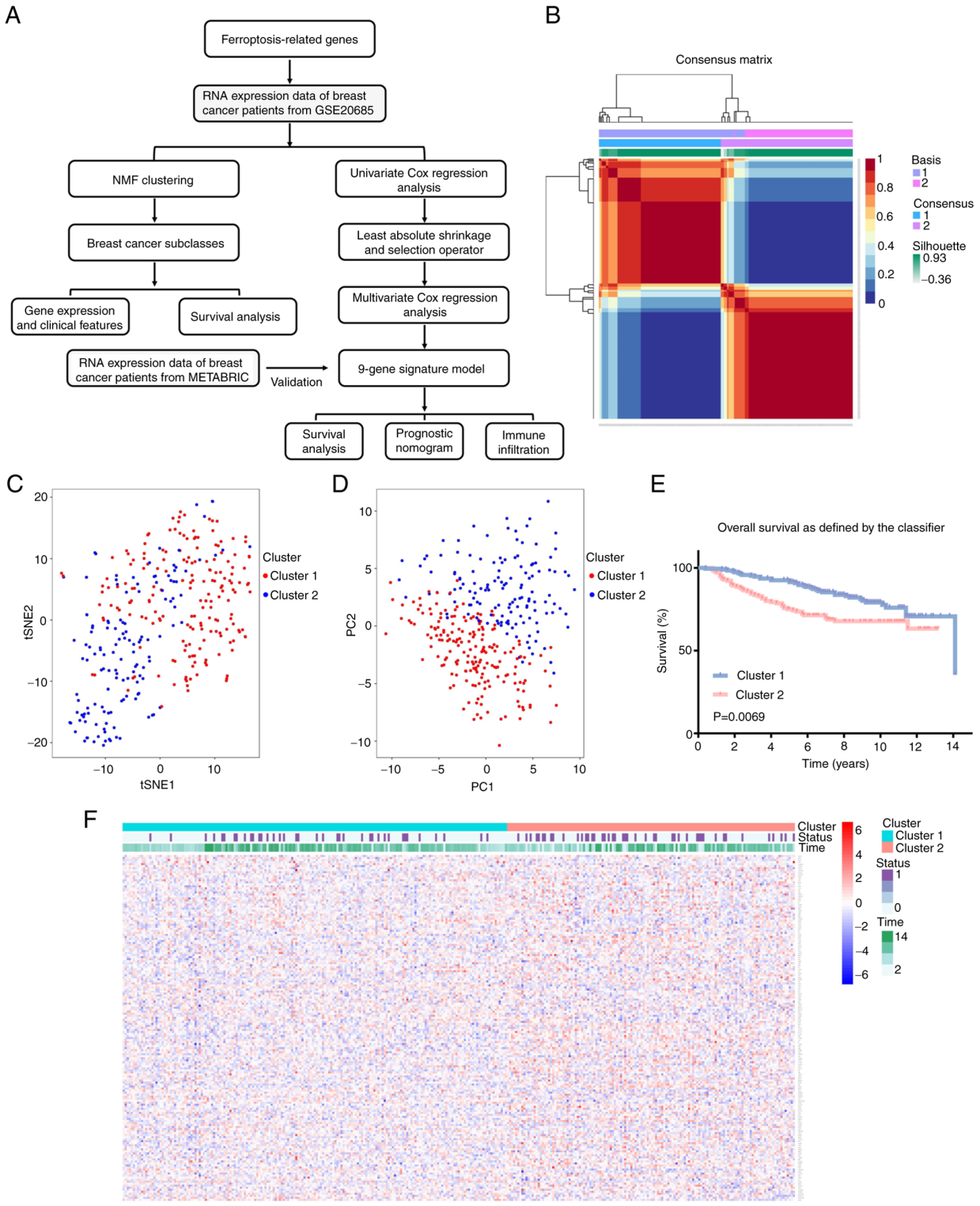

Figure 1. Identification of breast cancer subclasses using NMF consensus clustering in the ferroptosis set. (A) Flow chart of the study. (B) NMF clustering using 171 ferroptosis-related genes when k=2. (C) t-SNE analysis of the GSE20685 cohort. (D) Principal components analysis plot of the GSE20685 cohort. (E) Survival analysis of patients in clusters 1 and 2 in the GSE20685 cohort. (F) Heatmap showing the association between the expression of ferroptosis-related genes and the clinical status of the two clusters of patients with breast cancer. NMF, non-negative matrix factorization; t-SNE, T-distributed stochastic neighbor embedding; METABRIC, Molecular Taxonomy of Breast Cancer International Consortium.

The present study also evaluated the mRNA expression patterns of these FRGs in breast cancer according to METABRIC database. The expression of HILPDA, IFNG, MYB, DBN1, HES1, HSPB1 and SLC11A2 was significantly higher in breast cancer tissues compared with those in normal tissues. By contrast, the expression levels of YWHAE and CD44 were significantly reduced in breast cancer tissues as compared with in normal tissues (Fig. S2). These results indicated that several prognostic FRGs may serve an oncogenic role in breast cancer; however, the

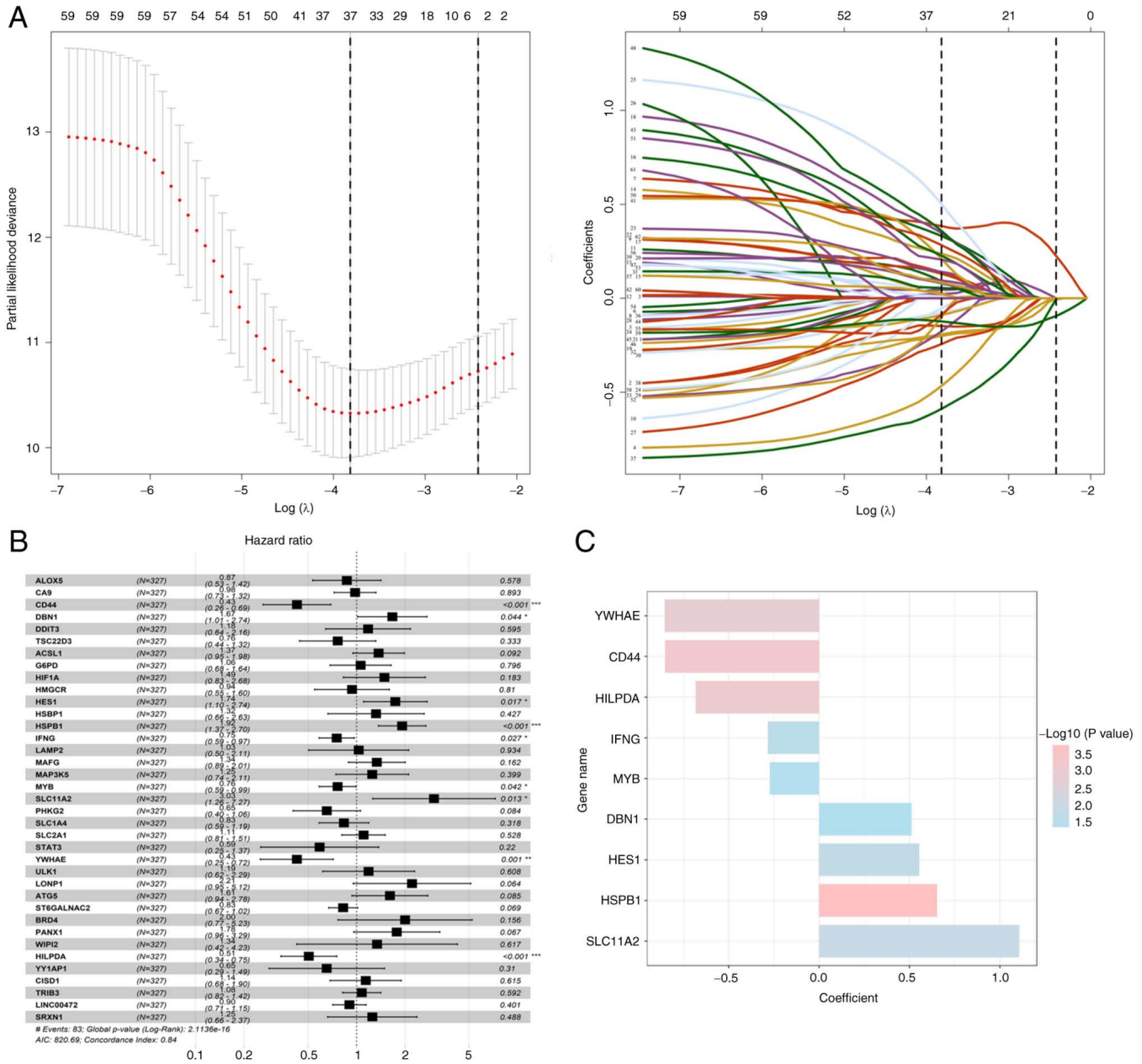

Figure 2. Identification of the FRGs closely associated with the prognosis of breast cancer. (A) LASSO Cox regression analysis was performed to construct the FRG-based risk score model. Partial likelihood deviance was determined by plotting the 10-fold cross-validation against the log (λ), and the optimal values are indicated by the two dotted vertical lines (left panel). The LASSO coefficient profiles of the 62 FRGs in breast cancer are indicated by the different colored curves (right panel). (B) Multiple Cox regression analysis. Forest plot of the associations between the expression of the FRGs and the survival of breast cancer. (C) Regression coefficients of the prognostic FRGs in breast cancer. FRG, ferroptosis-related gene; LASSO, least absolute shrinkage and selection operator.

specific mechanisms regulated by these genes require further study.

Comparison of immune infiltration between high-risk and low-risk patients with breast cancer. To evaluate the tumor heterogeneity between high-risk and low-risk groups, stromal score, immune score and tumor purity were calculated for both training and testing sets, using the ESTIMATE algorithm. The results indicated that the high-risk group exhibited higher tumor purity and lower immune score in the training and testing sets, whereas no significant differences were recorded between the stromal scores of the two groups (Fig. 5). In view of the significant differences recorded in the immune score for the two groups, the present study further evaluated immune infiltration patterns for the 22 immune cell types in the patients with breast cancer using the CIBERSORT algorithm. This may further aid in the characterization of the immunological landscape.

Patients with breast cancer belonging to the high-risk group exhibited higher ratios of M2 macrophages and resting mast cells, and lower ratios of memory B cells, CD8 T cells, T cells, activated CD4 memory T cells and resting NK cells in the GSE20685 cohort (Figs. 6A, S3A and B). Moreover, regulatory T cells (Tregs) were enriched in the high-risk group, whereas CD8 T cells, resting CD4 memory T cells, activated CD4 memory T cells, γδT cells, resting NK cells, activated NK

Table I. P-values and regression coefficients of the nine ferroptosis-related genes.

Gene	P-value	Coefficient
YWHAE	0.0013[b]	-0.854
CD44	0.0006[c]	-0.852
HILPDA	0.0008[c]	-0.683
IFNG	0.0268[a]	-0.284
MYB	0.0422[a]	-0.272
DBN1	0.0436[a]	0.511
HES1	0.0169[a]	0.554
HSPB1	0.0002[c]	0.652
SLC11A2	0.0133[a]	1.107

[a]P<0.05, [b]P<0.01, [c]P<0.001.

cells and activated mast cells were found to be enriched in the low-risk group in the METABRIC cohort (Fig. S3C and D). Although no significant differences were observed for M2 macrophages in the METABRIC cohort, the infiltration ratio was found to be relatively higher in the high-risk group compared with in the low-risk group. These results suggested that the poor prognosis of high-risk patients may be partly attributed to the immunosuppressive microenvironment.

To further analyze the immune status of the two groups, the ssGSEA algorithm was used to analyze the enrichment of additional types of immune cells, and related functions or pathways. The results of the analysis indicated that the high-risk group was associated with universally lower immune cell infiltration in the GSE20685 cohort (Figs. 6B and S3E). This was consistent with the lower immune scores recorded for the high-risk group. Moreover, the functions of antigen presentation, cytokine-cytokine receptor interaction, cytolytic activity, immune activation and immune surveillance were found to be at lower levels in the high-risk group (Figs. 6C and S3E). Comparative analysis in the METABRIC cohort confirmed the differences recorded for antigen-presenting cells, checkpoint molecules, macrophages, neutrophils and Treg cells between the two risk groups (Fig. S4A-C). The results of the study revealed that these FRGs may partly regulate tumor progression via modulation of the patterns of immune cell infiltration. However, further studies are needed to elucidate the underlying mechanisms.

Previous studies have reported the importance of checkpoint inhibitor-based immunotherapies (44,45). The results of the present study also revealed a substantial difference in the expression of several immune checkpoints between the high-risk and low-risk groups in the two cohorts (Figs. 7A, B, S5A and B). Considering abnormal immune infiltration patterns and differential expression of several immune checkpoint genes in the high-risk and low-risk groups, the study further assessed the probability of responding to immunotherapy. SubMap analysis was used to compare expression profiles of the two breast cancer sub-classes with a published dataset (40), which consisted of 47 patients with melanoma that were subjected to treatment involving programmed cell death protein-1 (PD-1) immune checkpoint inhibitor, or cytotoxic T-lymphocyte-associated protein-4 (CTLA-4) immune checkpoint inhibitor. The results of the SubMap analysis (46) indicated that the expression profile of the low-risk group was significantly correlated with the PD-1 response group (P=0.023976), which indicated that patients in the low-risk group would exhibit promising responses toward anti-PD-1 therapy (Fig. 7C).

Association between ferroptosis, proliferation, migration and drug resistance in breast cancer. Erastin, an inducer of ferroptosis, is known to bind and inhibit voltage-dependent anion channels (VDAC2/VDAC3) to trigger iron-dependent cell death (8). The present study further evaluated the effects of erastin on the development and progression of breast cancer. The results indicated that erastin treatment could inhibit breast cancer cell proliferation and promote the accumulation of ROS in a dose-dependent manner (Figs. 8A, B, S6A and B). Moreover, ferrostatin-1, a ferroptosis inhibitor, reversed the inhibition in cell viability and decreased ROS production induced by erastin (Figs. 8C, D, S6C and D). Furthermore, the migratory ability of breast cancer cells treated with vehicle or erastin was evaluated. When compared with vehicle-treated breast cancer cells, the migratory ability of erastin-treated breast cancer cells was inhibited. In comparison, ferrostatin-1 treatment could partially rescue the migratory ability of breast cancer cells (Figs. 8E and S6E). The present study also evaluated the effect of erastin on drug resistance of breast cancer cells. Notably, erastin treatment significantly increased the cytotoxicity of chemotherapeutics (paclitaxel and doxorubicin) and hormonal agents (tamoxifen). In comparison, ferrostatin-1 attenuated the activities of these drugs (Figs. 8F and S6F). These results indicated that erastin inhibited proliferation, migration and drug-resistance of breast cancer cells, which was mediated via induction of ferroptosis.

Novel treatment against FRGs in breast cancer. To screen potential molecular-targeted drugs for breast cancer, the present study further analyzed the correlation between the expression of FRGs and drug sensitivity on the basis of NCI-60 drug z-scores and gene expression profiling data of cancer cell lines obtained from the CellMiner database. The statistically significant correlations between the drug z-scores and gene expression (P<0.05) are listed in Table SIV. In general, a higher z-score is indicative of the higher sensitivity of the cells towards the corresponding drug. The representative Pearson's correlation dot plots are presented in Fig. S7. The drugs that were associated with at least four FRGs were selected for potential therapeutic regimens. Subsequently, seven FRG-related drugs were identified, which may be repurposed for breast cancer. The detailed information regarding correlation coefficients and drug applications obtained from DrugBank are listed in Table SV. In particular, nelarabine, which is known to be associated with MYB, HES1, SLC11A2, HILPDA and YWHAE, is used in acute T-cell lymphoblastic leukemia. This may be repurposed to treat breast cancer.

Discussion

Ferroptosis is a novel oxidative, iron-dependent form of cell death, which has attracted considerable attention in recent years. Previous studies have shown that regulation of

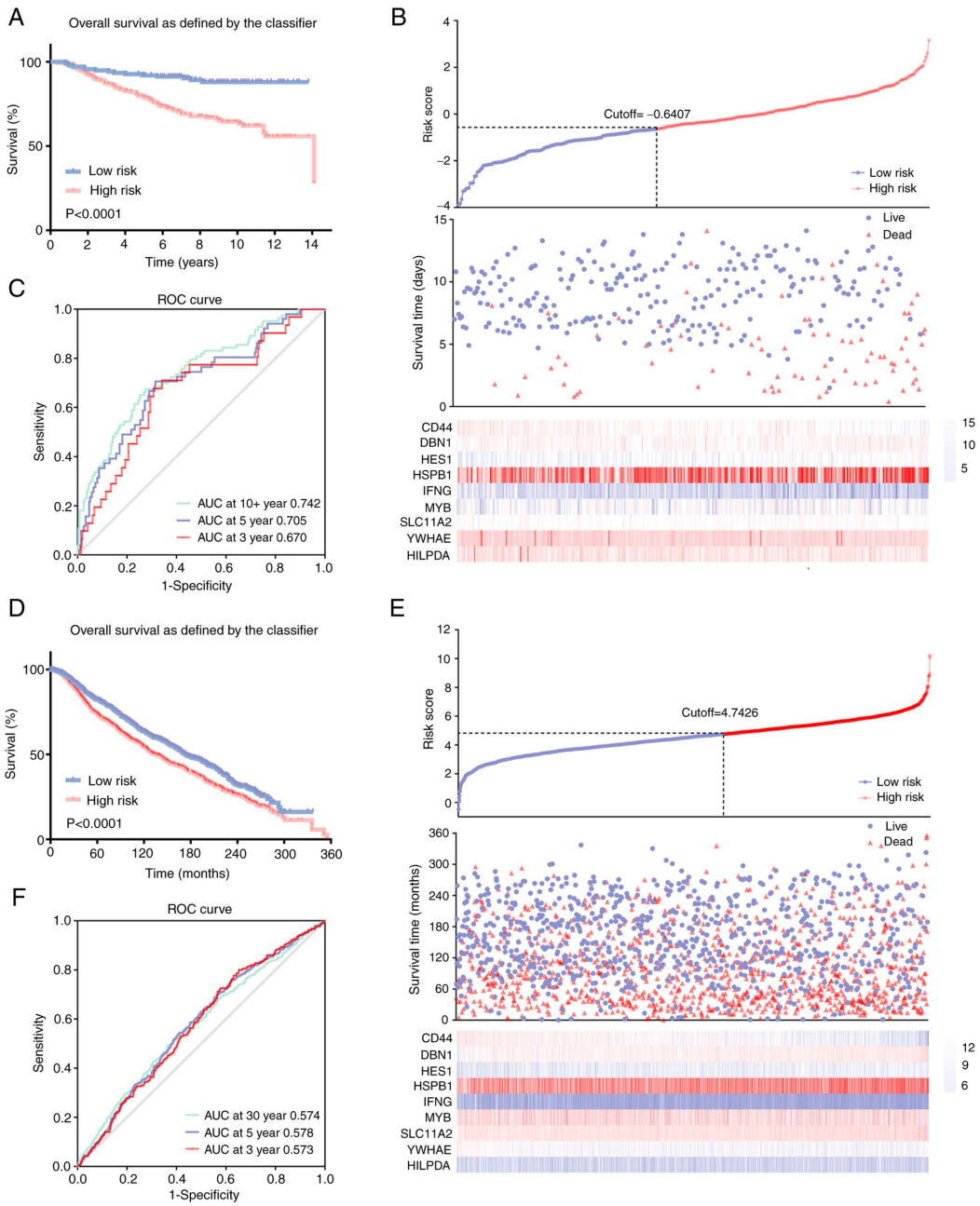

Figure 3. K-M survival analysis, risk score distribution and time-dependent ROC curves of the prognostic model in the patient data from GSE20685 and METABRIC cohorts. (A) K-M survival curves indicated that the OS in the high-risk group was markedly poorer than that in the low-risk group (P<0.001) in the GSE20685 database. (B) Distribution of risk scores under different gene expression characteristics in breast cancer in the GSE20685 database. (C) Time-dependent ROC curve analysis measuring the predictive performance on OS in the GSE20685 database. (D) K-M survival curves indicated that the OS in the high-risk group was markedly poorer than that in the low-risk group (P<0.001) in the METABRIC database. (E) Distribution of risk scores under different gene expression characteristics in breast cancer in the METABRIC database. (F) Time-dependent ROC curve analysis measuring the predictive performance on OS in the METABRIC database. K-M, Kaplan-Meier; OS, overall survival; ROC, receiver operating characteristics; AUC, area under the curve; METABRIC, Molecular Taxonomy of Breast Cancer International Consortium.

ferroptosis can modulate cell proliferation, migration and drug resistance in various types of cancer (47,48). Additionally, it has been shown to serve a crucial role in tumor progression and cancer therapeutics. However, the role of ferroptosis in breast cancer has not been fully elucidated. The present study systematically investigated the expression of FRGs, and analyzed their association with OS and immune infiltration in breast cancer.

Several prognostic models based on FRG signatures have been constructed to explore prognosis-related biomarkers and predict the prognosis of various types of cancer. A previous study developed a 13-gene prognostic model (49), wherein AUCs were recorded to be 0.819, 0.815 and 0.891 for 1-, 3- and 5-year survival rates of patients with acute myeloid leukemia. In another study, five FRGs were used to construct a prognostic model with an AUC of 0.816, and the nomogram exhibited good performance in the prediction of 3-year survival rate of patients with thyroid cancer (50). However, the effect of FRGs in prognostic prediction for patients with breast cancer has not been fully evaluated. The present study

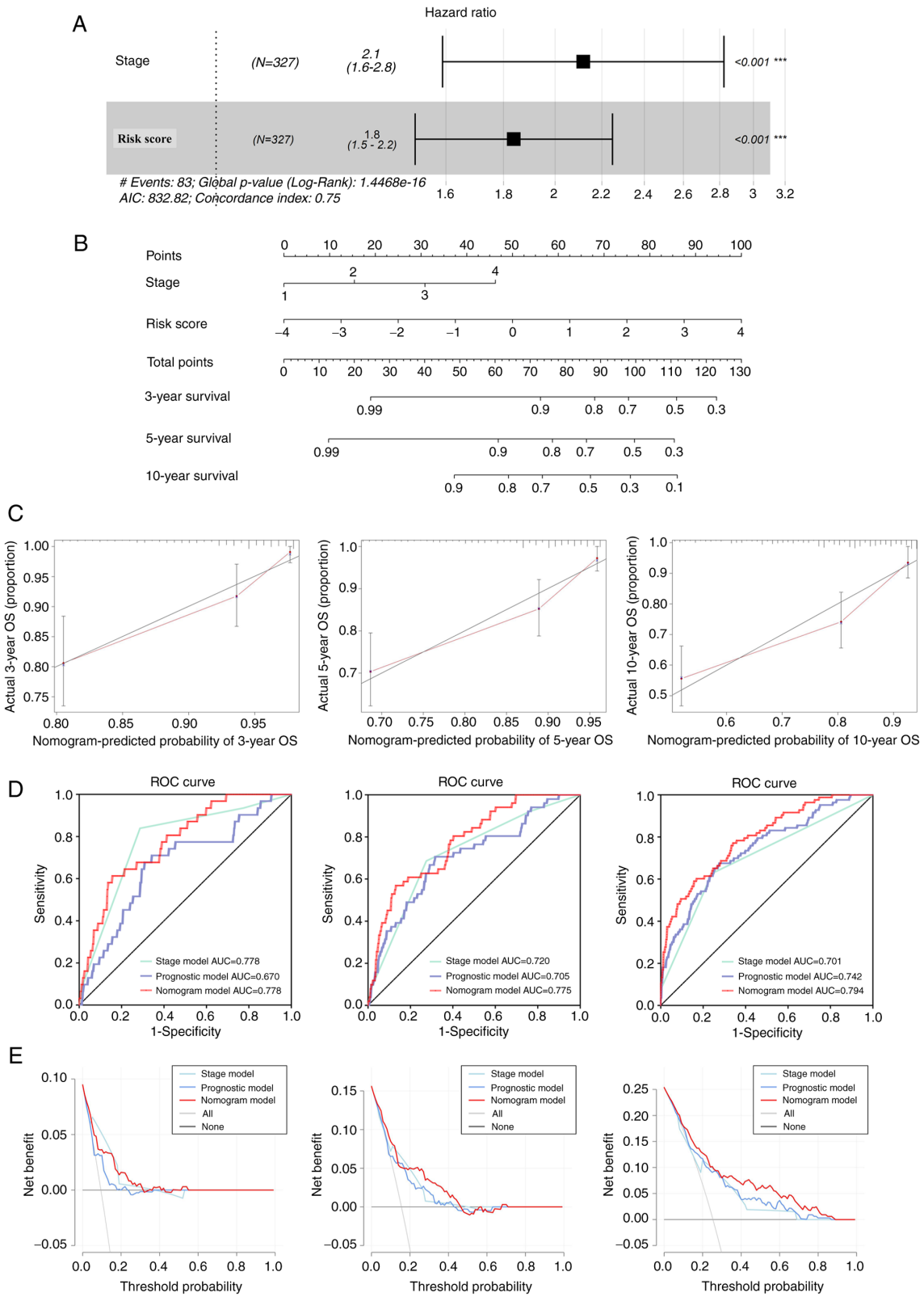

Figure 4. Construction and validation of the predictive nomogram. (A) Univariate and multivariate Cox regression analysis confirmed that the prognostic signature and TNM stage were independent prognostic predictors. (B) Nomogram for predicting the OS of patients with breast cancer at 3, 5 and 10 years. (C) Calibration curves of the nomogram for OS prediction at 3, 5 and 10 years. (D) ROC curves to evaluate the predictive ability of the nomogram. (E) Decision curve analysis determined that the nomogram could obtain the optimal net benefit at 3, 5 and 10 years. OS, overall survival; ROC, receiver operating characteristic; AUC, area under the curve.

established a ferroptosis-related prognostic model of breast cancer based on the GSE20685 database and the model was further validated using data from the METABRIC database. Moreover, the results for univariate, LASSO and multivariate regression analyses assisted in the identification of a novel prognostic model that consisted of nine FRGs. The nine-FRG

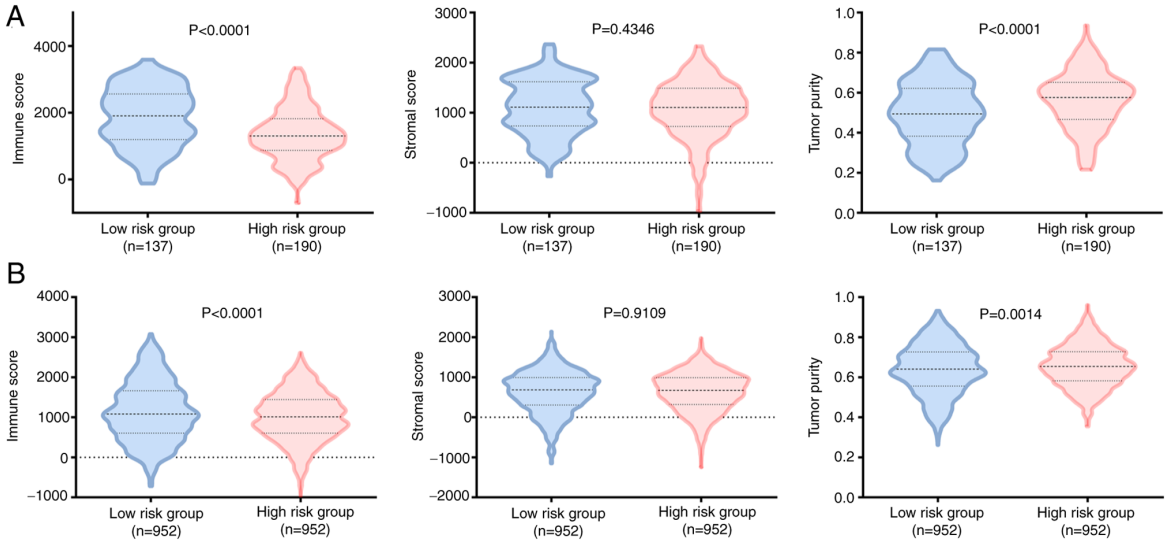

Figure 5. ESTIMATE analyses in the high-risk and low-risk groups. Violin plots of the immune score, stromal score and tumor purity from the ESTIMATE analysis of the two groups in the (A) GSE20685 and (B) METABRIC datasets. For violin plots, the three lines within the boxes represent the 25th percentile, median value and the 75th percentile. The bottom and top of the plots represent the minimum and maximum values. ESTIMATE, estimation of stromal and immune cells in malignant tumor tissues using expression data; METABRIC, Molecular Taxonomy of Breast Cancer International Consortium.

prognostic model classified patients with breast cancer into high-risk and low-risk groups. Survival analysis demonstrated that prognosis of patients included in the high-risk group was poorer compared with that in the low-risk group. ROC analysis further confirmed the accuracy and sensitivity of the gene signature. It has previously been reported that the clinicopathological parameters age and TNM stage are commonly used for clinical decision-making and prognostic prediction in breast cancer (51). These clinical features were included in the present study to perform univariate and multivariate regression analysis, and the results indicated that TNM stage and risk score acted as independent prognostic indicators for OS. Subsequently, a novel prognostic nomogram was constructed based on these two parameters, to estimate 3-, 5- and 10-year survival rates in patients with breast cancer. The AUCs of the nomogram were recorded to be higher than those of FRGs or the TNM stage alone, which was suggestive of the stability and reliability of the nomogram in the prediction of the survival rate in patients with breast cancer. AUCs were recorded to be 0.778, 0.775 and 0.794 with the nomogram for 3-, 5- and 10-year OS, respectively, which had a higher predictive effect for breast cancer than a single factor. However, given the incompleteness of the clinical information obtained, the predictive nomogram was not further validated in the validation dataset. A previous study also used similar methods and did not validate the nomogram in the validation dataset, demonstrating the feasibility and validity of the present study (14). These results indicated that the nine-FRGs prognostic model served as a reliable prognostic indicator for patients with breast cancer.

The prognostic model consisted of nine FRGs that could be roughly classified as protective factors (YWHAE, CD44, HILPDA, IFNG and MYB) and risk factors (DBN1, HES1, HSPB1 and SLC11A2) based on their regression coefficients for breast cancer prognosis. YWHAE is a member of the 14-3-3 protein family, which serves as a marker of ferroptosis. A previous study reported that YWHAE was overexpressed in breast cancer tissues, and its expression was associated with poor survival, which could further promote cancer progression and chemoresistance in breast cancer cells (52). CD44, a key marker of cancer stemness, has previously been reported to be negatively associated with ferroptosis. In a previous study, CD44 overexpression promoted the stability of SLC7A11, by enhancing the interaction between SLC7A11 and OTUB1, which in turn resulted in the suppression of ferroptosis in lung carcinoma cells (53). HILPDA is known to be an important driver of ferroptosis for clear-cell carcinoma, which can enrich polyunsaturated lipids and promote ferroptosis sensitivity downstream of HIF-2α (54). IFNG, released from immunotherapy-activated $CD8^+$ T cells or radiotherapy-activated ATM, can downregulate the expression of SLC3A2 and SLC7A11, which can further assist in the promotion of lipid peroxidation and ferroptosis that improve tumor control (27,55). MYB is a well-known transcription factor, which has a critical role in cellular metabolism (56,57), including fatty acid metabolism, glucose-induced oxidative stress and cysteine metabolism. It has been reported that MYB can transcriptionally upregulate CDO1, which can result in a decrease in GPX4 expression, leading to increased ferroptosis (58). Although the expression of partial protective factors was reported to be upregulated in breast cancer tissues in some studies, their expression levels may be inconsistent with other databases or cohorts, and the detailed role in breast cancer progression requires further exploration. Based on a series of integrated analysis, the aforementioned five genes were considered as potential protective factors in the present study, which may draw a different conclusion from the analysis based on single factors. In terms of risk factors, DBN1 is an actin-binding protein, which acts as a ferroptosis regulator in pancreatic cancer (32). High DBN1 expression has been reported to be significantly associated with a poorer prognosis and drug resistance in various types of cancer (59), including lung adenocarcinoma and breast cancer. Elevated

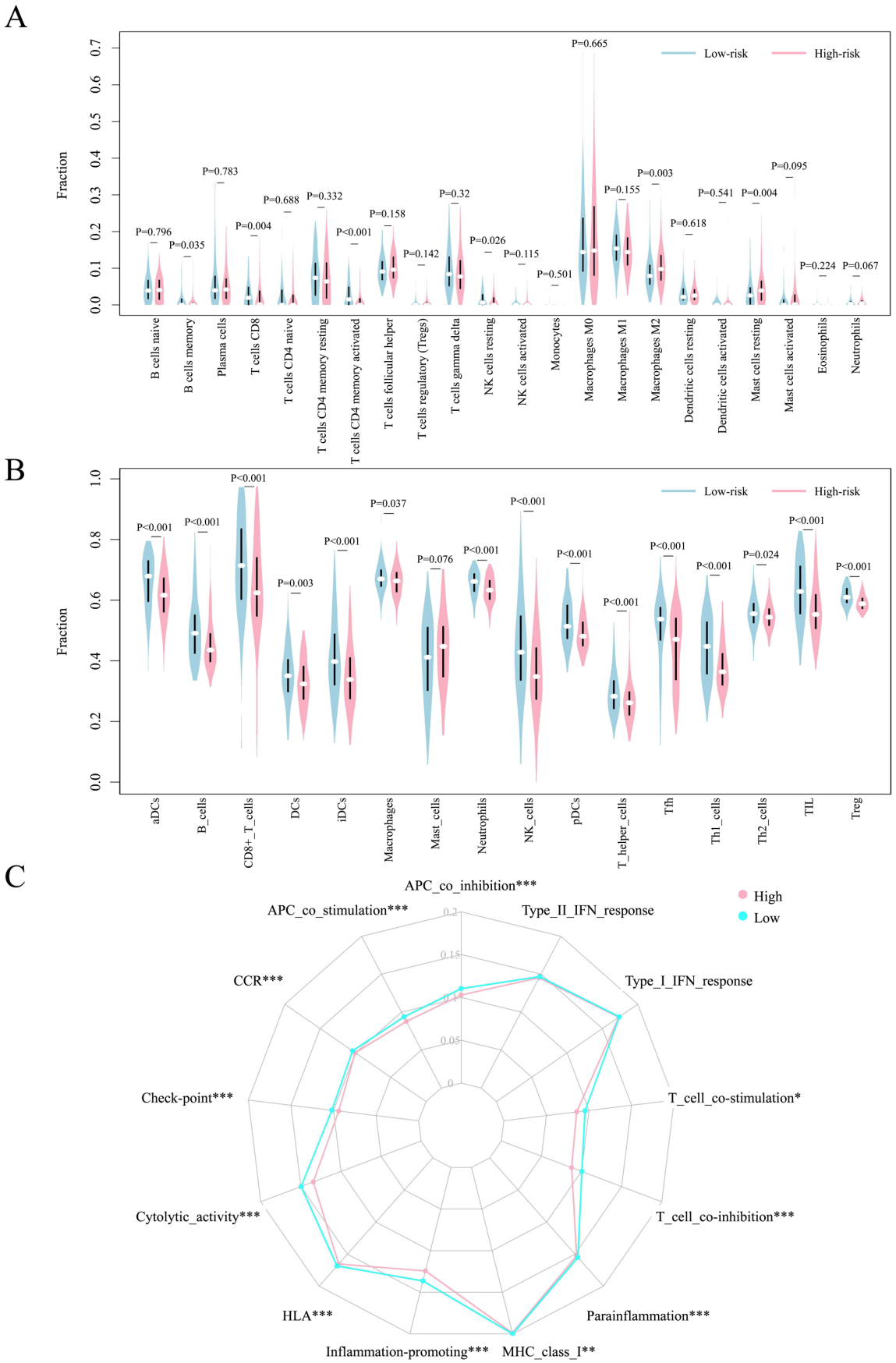

Figure 6. Immune infiltration in patients with breast cancer with different risk scores based on the CIBERSORT and ssGSEA algorithms. (A) Violin plots were used to visualize the fractions of different immune cells in the high-risk and low-risk groups in the GSE20685 cohort. (B) Violin plots were used to visualize the fractions of 16 immune cells in the high-risk and low-risk groups in the GSE20685 cohort. (C) Radar maps were used to visualize the scores of 13 immune-related functions in the high-risk and low-risk groups in the GSE20685 cohort. *P<0.05, **P<0.01, ***P<0.001, high risk group vs. low risk group. ssGSEA, single-sample gene set enrichment analysis.

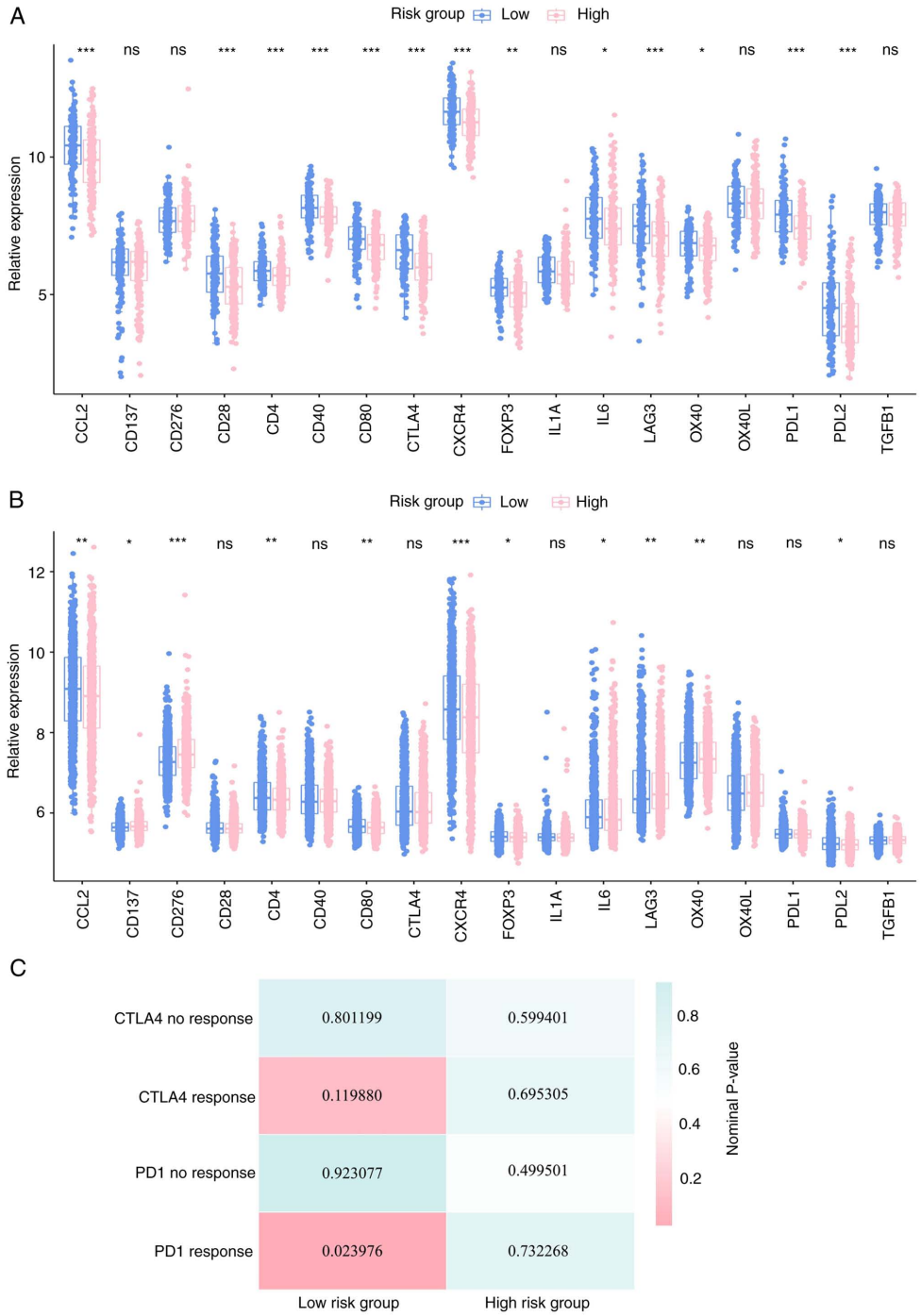

Figure 7. Expression of immune checkpoint genes in patients with breast cancer with different risk scores. Box plots showing the expression of several immune checkpoint genes in the high-risk and low-risk groups in the (A) GSE20685 and (B) METABRIC cohorts. (C) SubMap analysis for immunotherapeutic prediction in the training set. The nominal P-value is indicated by the color-coded bar, where pink refers to a smaller nominal P-value and green refers to a larger nominal P-value. METABRIC, Molecular Taxonomy of Breast Cancer International Consortium. *P<0.05, **P<0.01, ***P<0.001, high risk group vs. low risk group.

HES1 expression has also been previously reported in multiple types of cancer, including ovarian cancer (60), non-small cell lung cancer (61) and breast cancer (62). Moreover, it was observed that high expression of HES1 was associated with a poorer prognosis in patients with breast cancer, and HES1 overexpression resulted in enhanced proliferation, invasion and stemness in breast cancer (62,63). HSPB1 is a member of the small heat shock family of proteins, which can be induced by erastin treatment in an HSF1-dependent manner in various cancer cells. In particular, HSPB1 can reduce cellular iron uptake and lipid ROS production, whereas HSPB1 knockdown has been shown to result in enhancement of erastin-induced ferroptosis (64). SLC11A2 is a proton-dependent iron importer of Fe^{2+}, which has previously been shown to be physiologically important for cellular uptake of iron. A previous study reported higher expression of SLC11A2 in MCF-7 cells compared with in MCF-12A cells (65). Notably, the present study revealed that most of these prognostic FRGs were differentially expressed between breast cancer tissues and normal tissues; however, classical FRGs, such as ACSL4 and GPX4,

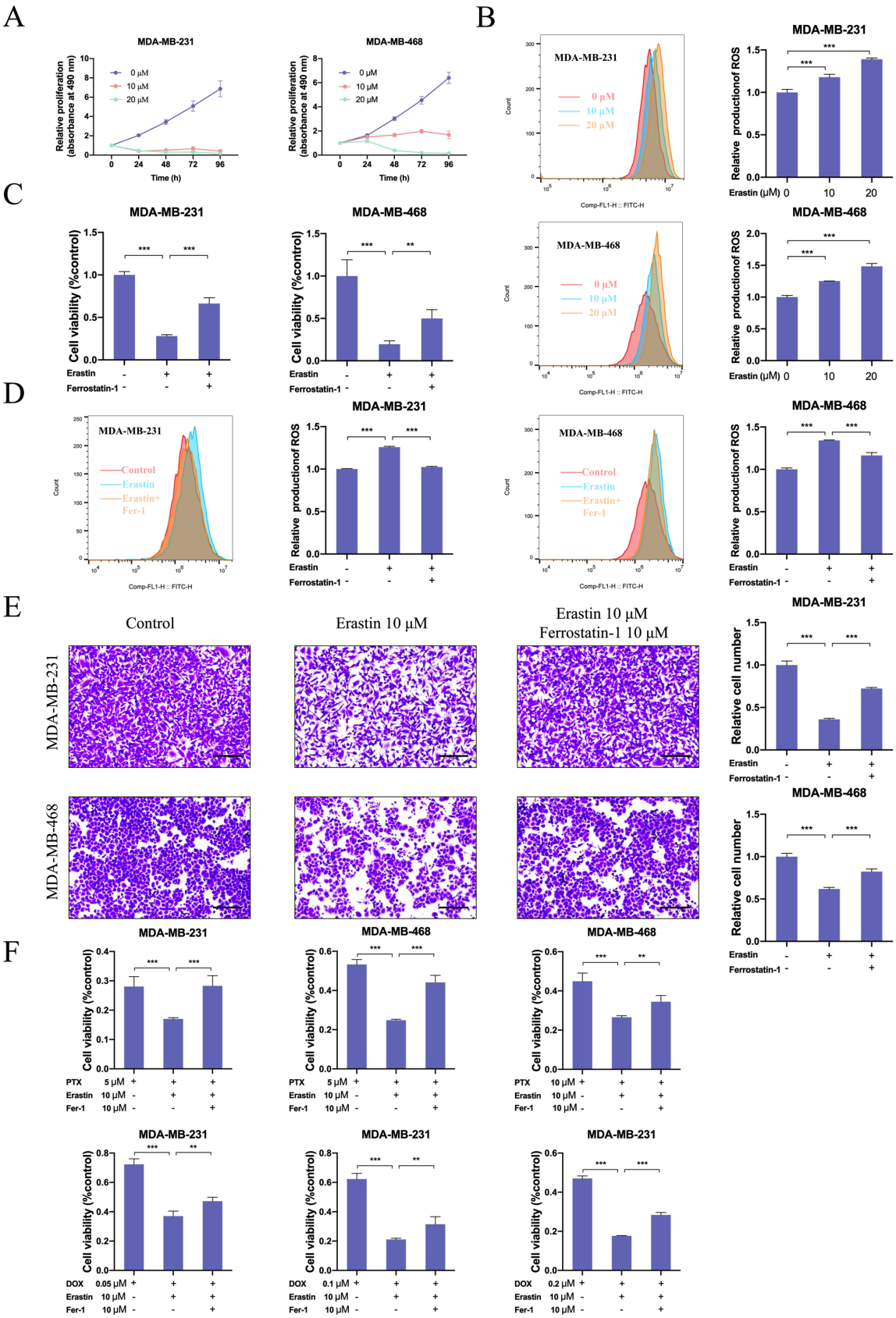

Figure 8. Erastin treatment suppresses proliferation, migration and drug resistance of breast cancer cells. Cells were treated with 10 or 20 μM erastin. Erastin treatment inhibited the (A) proliferation and (B) enhanced ROS accumulation in MDA-MB-231 and MDA-MB-468 cells in a dose-dependent manner. Cells were treated with 10 μM erastin with or without 10 μM ferrostatin-1. Ferrostatin-1 (C) attenuated the suppression of cell proliferation and (D) reduced the production of ROS induced by erastin. (E) Cells were treated with 10 μM erastin with or without 10 μM ferrostatin-1. Erastin treatment decreased the migratory ability of breast cancer cells relative to those of vehicle-treated cells, and ferrostatin-1 attenuated the suppression in cell migration induced by erastin. Scale bar, 200 μm. (F) Cells were treated with 10 μM erastin with or without 10 μM ferrostatin-1, PTX or DOX (indicated concentrations). Erastin treatment enhanced the chemotherapeutic-induced cell death, whereas ferrostatin-1 attenuated the inhibitory effect of erastin on cell viability. **P<0.01, ***P<0.001. ROS, reactive oxygen species; PTX, paclitaxel; DOX, doxorubicin.

were not included in the FRGs model. It was hypothesized that on the one hand, ACSL4 and GPX4 may have little independent prognostic value, independent of the FRGs model. On the other hand, genes in the FRGs model are potentially upstream and downstream of the key ferroptosis genes, partly replacing the functions of the key ferroptosis genes in the model for breast cancer. Therefore, in general, as crucial components associated with tumor progression or modulating treatment sensitivity, these nine FRGs have considerable potential as therapeutic targets or biomarkers in breast cancer.

Immunotherapy, involving immune checkpoint inhibitors, cyclin-dependent kinase inhibitors and dendritic cell vaccines, is widely applied in the treatment of various types of cancer (66). However, it has been reported that immunosuppressive mechanisms may be initiated during the development and progression of several types of cancer, to circumvent antitumor immune responses (67). These immunosuppressive mechanisms include the increased infiltration of immunosuppressive cells and molecules, and the enrichment of low-immunogenic cancer cells. The results of the present study obtained from the two datasets revealed that there was a considerable difference in the types of immune cells and the infiltration ratio of immune cells between high-risk and low-risk groups, indicating that the FRGs may regulate tumor progression partly via modulation of the patterns of immune cell infiltration. The low-risk group exhibited a higher immune score, and it was enriched with multiple immune cells and immune-related pathways. This further indicated that patients in the low-risk group may exhibit a better immune status and immune function. Notably, a higher proportion of M2 macrophages and Treg cells indicated that a stronger immunosuppressive effect may be responsible for the poor prognosis in the high-risk group. Moreover, increased expression of several immune checkpoints indicated that patients in the low-risk group may benefit more from immune checkpoint inhibitors, as indicated by the SubMap analysis. Previous studies have also highlighted the promising role of ferroptosis in cancer immunotherapy. In particular, GPX4 may facilitate activation of stimulator-of-interferon genes, which can further promote the initiation of an innate immune response against microbial infection and tumors (68). $CD8^+$ T cells have been reported to enhance sensitization towards ferroptosis, via secretion of IFNγ in cancer cells (27). Therefore, targeting the tumor ferroptosis pathway in combination with immunotherapy may serve as a novel therapeutic strategy for cancer management. However, further investigation is required to elucidate the immunomodulatory role of ferroptosis in antitumor immunity.

Erastin is a classical inducer of ferroptosis, which can directly bind to VDAC2/VDAC3 to alter the permeability of the outer mitochondrial membrane, thus leading to a decreased rate of NADH oxidation and increased ROS production, thereby inducing ferroptosis (69,70). The present study revealed that erastin treatment could inhibit the proliferation and migration of breast cancer cells, which was mediated via induction of ferroptosis. Notably, these effects could be attenuated by ferrostatin-1 treatment. It has previously been reported that resistance to chemotherapeutics can result in therapeutic failure and a poor prognosis in patients with breast cancer (71). The present study demonstrated that erastin treatment could increase the sensitivity of breast cancer cells towards chemotherapeutics and hormonal agents, which indicated that a ferroptosis inducer may be used as a potential combinatorial treatment strategy for the treatment of breast cancer. The underlying mechanisms responsible for drug sensitivity should be investigated in the future.

The present study has some limitations. First, with the continuous advances in ferroptosis research, an increasing number of FRGs may be identified and analyzed in the future, leading to different analysis results and prognostic models. Second, limited by the clinical information available in the databases used, stratification analysis by molecular subtypes, therapies or clinical stage could not be performed. Third, the predictive model needs to be validated in large-scale studies before application in clinical practice. Fourth, non-tumor cell lines were not used to evaluate the cytotoxicity of the ferroptosis inducer. Finally, future *in vivo* and *in vitro* studies need to be conducted to validate the study, and further explore the specific function and mechanism of genes in the model.

In conclusion, the present study identified a novel prognostic model based on nine FRGs. This model could independently predict the prognosis of patients with breast cancer. In addition, the present study provided novel insights into the roles of ferroptosis in the progression and treatment of breast cancer, and revealed an important avenue that may be utilized for the treatment of breast cancer. Further investigations are required to elucidate the functional roles and underlying mechanisms of these FRGs in breast cancer.

Acknowledgements

Not applicable.

Funding

This work was supported by the National Key Research and Development Program (grant no. 2020YFA0712400), the Special Foundation for Taishan Scholars (grant no. ts20190971) and the National Natural Science Foundation of China (grant nos. 81874119, 81902695, 82072912, and 82002785).

Availability of data and materials

The datasets used were obtained from the Gene Expression Omnibus (accession no. GSE20685, https://www.ncbi.nlm.nih.gov/geo/) and METABRIC databases (downloaded from cBioPortal, https://www.cbioportal.org/). The data used for prediction of potential drugs was obtained from the CellMiner and DrugBank databases. The other datasets used and/or analyzed during the current study are available from the corresponding author on reasonable request.

Authors' contributions

YZ and QY conceived and designed the experiments. YZ, YL, YW, FY and XK performed the experiments and analyzed the data. YZ and QY wrote and revised the manuscript. YZ and YL confirm the authenticity of all the raw data. All authors read and approved the final manuscript.

Ethics approval and consent to participate

Not applicable.

Patient consent for publication

Not applicable.

Competing interests

The authors declare that they have no competing interests.

References

1. Radenkovic S, Konjevic G, Isakovic A, Stevanovic P, Gopcevic K and Jurisic V: HER2-positive breast cancer patients: Correlation between mammographic and pathological findings. Radiat Prot Dosimetry 162: 125-128, 2014.
2. Bray F, Ferlay J, Soerjomataram I, Siegel RL, Torre LA and Jemal A: Global cancer statistics 2018: GLOBOCAN estimates of incidence and mortality worldwide for 36 cancers in 185 countries. CA Cancer J Clin 68: 394-424, 2018.
3. Tao Z, Shi A, Lu C, Song T, Zhang Z and Zhao J: Breast cancer: Epidemiology and etiology. Cell Biochem Biophys 72: 333-338, 2015.
4. Feng Y, Spezia M, Huang S, Yuan C, Zeng Z, Zhang L, Ji X, Liu W, Huang B, Luo W, *et al*: Breast cancer development and progression: Risk factors, cancer stem cells, signaling pathways, genomics, and molecular pathogenesis. Genes Dis 5: 77-106, 2018.
5. Radenkovic S, Konjevic G, Gavrilovic D, Stojanovic-Rundic S, Plesinac-Karapandzic V, Stevanovic P and Jurisic V: pSTAT3 expression associated with survival and mammographic density of breast cancer patients. Pathol Res Pract 215: 366-372, 2019.
6. Chen F, Han B, Meng Y, Han Y, Liu B, Zhang B, Chang Y, Cao P, Fan Y and Tan K: Ceruloplasmin correlates with immune infiltration and serves as a prognostic biomarker in breast cancer. Aging (Albany NY) 13: 20438-20467, 2021.
7. Lee SY, Ju MK, Jeon HM, Jeong EK, Lee YJ, Kim CH, Park HG, Han SI and Kang HS: Regulation of tumor progression by programmed necrosis. Oxid Med Cell Longev 2018: 3537471, 2018.
8. Dixon SJ, Lemberg KM, Lamprecht MR, Skouta R, Zaitsev EM, Gleason CE, Patel DN, Bauer AJ, Cantley AM, Yang WS, *et al*: Ferroptosis: An iron-dependent form of nonapoptotic cell death. Cell 149: 1060-1072, 2012.
9. Seibt TM, Proneth B and Conrad M: Role of GPX4 in ferroptosis and its pharmacological implication. Free Radic Biol Med 133: 144-152, 2019.
10. Yuan H, Li X, Zhang X, Kang R and Tang D: CISD1 inhibits ferroptosis by protection against mitochondrial lipid peroxidation. Biochem Biophys Res Commun 478: 838-844, 2016.
11. Dodson M, Castro-Portuguez R and Zhang DD: NRF2 plays a critical role in mitigating lipid peroxidation and ferroptosis. Redox Biol 23: 101107, 2019.
12. Ooko E, Saeed ME, Kadioglu O, Sarvi S, Colak M, Elmasaoudi K, Janah R, Greten HJ and Efferth T: Artemisinin derivatives induce iron-dependent cell death (ferroptosis) in tumor cells. Phytomedicine 22: 1045-1054, 2015.
13. Wu ZH, Tang Y, Yu H and Li HD: The role of ferroptosis in breast cancer patients: A comprehensive analysis. Cell Death Discov 7: 93, 2021.
14. Wang D, Wei G, Ma J, Cheng S, Jia L, Song X, Zhang M, Ju M, Wang L, Zhao L, *et al*: Identification of the prognostic value of ferroptosis-related gene signature in breast cancer patients. BMC Cancer 21: 645, 2021.
15. Sato M, Kusumi R, Hamashima S, Kobayashi S, Sasaki S, Komiyama Y, Izumikawa T, Conrad M, Bannai S and Sato H: The ferroptosis inducer erastin irreversibly inhibits system xc- and synergizes with cisplatin to increase cisplatin's cytotoxicity in cancer cells. Sci Rep 8: 968, 2018.
16. Guo J, Xu B, Han Q, Zhou H, Xia Y, Gong C, Dai X, Li Z and Wu G: Ferroptosis: A novel anti-tumor action for cisplatin. Cancer Res Treat 50: 445-460, 2018.
17. Li Z, Chen L, Chen C, Zhou Y, Hu D, Yang J, Chen Y, Zhuo W, Mao M, Zhang X, *et al*: Targeting ferroptosis in breast cancer. Biomark Res 8: 58, 2020.
18. Xie Y, Xiao Y, Liu Y, Lu X, Wang Z, Sun S, Liu L, Tang X, Xiao H and Liu H: Construction of a novel radiosensitivity- and ferroptosis-associated gene signature for prognosis prediction in gliomas. J Cancer 13: 2683-2693, 2022.
19. Yue Z, Sun J and Shi L: Construction and validation of a 6-Ferroptosis related gene signature for prognosis and immune landscape prediction in melanoma. Front Genet 13: 887542, 2022.
20. Xing XL, Liu Y, Liu J, Zhou H, Zhang H, Zuo Q, Bu P, Duan T, Zhou Y and Xiao Z: Comprehensive analysis of ferroptosis- and immune-related signatures to improve the prognosis and diagnosis of kidney renal clear cell carcinoma. Front Immunol 13: 851312, 2022.
21. Sui S, Xu S and Pang D: Emerging role of ferroptosis in breast cancer: New dawn for overcoming tumor progression. Pharmacol Ther 232: 107992, 2022.
22. Wu M, Zhang X, Zhang W, Chiou YS, Qian W, Liu X, Zhang M, Yan H, Li S, Li T, *et al*: Cancer stem cell regulated phenotypic plasticity protects metastasized cancer cells from ferroptosis. Nat Commun 13: 1371, 2022.
23. Konjevic GM, Vuletić AM, Mirjacic Martinovic KM, Larsen AK and Jurisic VB: The role of cytokines in the regulation of NK cells in the tumor environment. Cytokine 117: 30-40, 2019.
24. Jurisic V: Multiomic analysis of cytokines in immuno-oncology. Expert Rev Proteomics 17: 663-674, 2020.
25. Ni S, Yuan Y, Kuang Y and Li X: Iron metabolism and immune regulation. Front Immunol 13: 816282, 2022.
26. Ganz T and Nemeth E: Iron homeostasis in host defence and inflammation. Nat Rev Immunol 15: 500-510, 2015.
27. Wang W, Green M, Choi JE, Gijon M, Kennedy PD, Johnson JK, Liao P, Lang X, Kryczek I, Sell A, *et al*: $CD8^+$ T cells regulate tumour ferroptosis during cancer immunotherapy. Nature 569: 270-274, 2019.
28. Kao KJ, Chang KM, Hsu HC and Huang AT: Correlation of microarray-based breast cancer molecular subtypes and clinical outcomes: Implications for treatment optimization. BMC Cancer 11: 143, 2011.
29. Curtis C, Shah SP, Chin SF, Turashvili G, Rueda OM, Dunning MJ, Speed D, Lynch AG, Samarajiwa S, Yuan Y, *et al*: The genomic and transcriptomic architecture of 2,000 breast tumours reveals novel subgroups. Nature 486: 346-352, 2012.
30. Wu Q, Tang X, Zhu W, Li Q, Zhang X and Li H: The potential prognostic role of oligosaccharide-binding fold-containing protein 2A (OBFC2A) in triple-negative breast cancer. Front Oncol 11: 751430, 2021.
31. Zhuo S, Chen Z, Yang Y, Zhang J, Tang J and Yang K: Clinical and biological significances of a ferroptosis-related gene signature in glioma. Front Oncol 10: 590861, 2020.
32. Tang R, Hua J, Xu J, Liang C, Meng Q, Liu J, Zhang B, Yu X and Shi S: The role of ferroptosis regulators in the prognosis, immune activity and gemcitabine resistance of pancreatic cancer. Ann Transl Med 8: 1347, 2020.
33. R Core Team (2012). R: A language and environment for statistical computing. R Foundation for Statistical Computing, Vienna, Austria. ISBN 3-900051-07-0, URL http://www.R-project.org/.
34. Gaujoux R and Seoighe C: A flexible R package for nonnegative matrix factorization. BMC Bioinformatics 11: 367, 2010.
35. Brunet JP, Tamayo P, Golub TR and Mesirov JP: Metagenes and molecular pattern discovery using matrix factorization. Proc Natl Acad Sci USA 101: 4164-4169, 2004.
36. Friedman J, Hastie T and Tibshirani R: Regularization paths for generalized linear models via coordinate descent. J Stat Softw 33: 1-22, 2010.
37. Yoshihara K, Shahmoradgoli M, Martinez E, Vegesna R, Kim H, Torres-Garcia W, Trevino V, Shen H, Laird PW, Levine DA, *et al*: Inferring tumour purity and stromal and immune cell admixture from expression data. Nat Commun 4: 2612, 2013.
38. Becht E, Giraldo NA, Lacroix L, Buttard B, Elarouci N, Petitprez F, Selves J, Laurent-Puig P, Sautes-Fridman C, Fridman WH, *et al*: Estimating the population abundance of tissue-infiltrating immune and stromal cell populations using gene expression. Genome Biol 17: 218, 2016.
39. Rooney MS, Shukla SA, Wu CJ, Getz G and Hacohen N: Molecular and genetic properties of tumors associated with local immune cytolytic activity. Cell 160: 48-61, 2015.

40. Roh W, Chen PL, Reuben A, Spencer CN, Prieto PA, Miller JP, Gopalakrishnan V, Wang F, Cooper ZA, Reddy SM, *et al*: Integrated molecular analysis of tumor biopsies on sequential CTLA-4 and PD-1 blockade reveals markers of response and resistance. Sci Transl Med 9: eaah3560, 2017.
41. Reinhold WC, Sunshine M, Liu H, Varma S, Kohn KW, Morris J, Doroshow J and Pommier Y: CellMiner: A web-based suite of genomic and pharmacologic tools to explore transcript and drug patterns in the NCI-60 cell line set. Cancer Res 72: 3499-3511, 2012.
42. Ritchie ME, Phipson B, Wu D, Hu Y, Law CW, Shi W and Smyth GK: limma powers differential expression analyses for RNA-sequencing and microarray studies. Nucleic Acids Res 43: e47, 2015.
43. Vickers AJ, Cronin AM, Elkin EB and Gonen M: Extensions to decision curve analysis, a novel method for evaluating diagnostic tests, prediction models and molecular markers. BMC Med Inform Decis Mak 8: 53, 2008.
44. Michielin O, Lalani AK, Robert C, Sharma P and Peters S: Defining unique clinical hallmarks for immune checkpoint inhibitor-based therapies. J Immunother Cancer 10: e003024, 2022.
45. Hubert P, Roncarati P, Demoulin S, Pilard C, Ancion M, Reynders C, Lerho T, Bruyere D, Lebeau A, Radermecker C, *et al*: Extracellular HMGB1 blockade inhibits tumor growth through profoundly remodeling immune microenvironment and enhances checkpoint inhibitor-based immunotherapy. J Immunother Cancer 9: e001966, 2021.
46. Yang C, Huang X, Liu Z, Qin W and Wang C: Metabolism-associated molecular classification of hepatocellular carcinoma. Mol Oncol 14: 896-913, 2020.
47. Wang M, Mao C, Ouyang L, Liu Y, Lai W, Liu N, Shi Y, Chen L, Xiao D, Yu F, *et al*: Long noncoding RNA LINC00336 inhibits ferroptosis in lung cancer by functioning as a competing endogenous RNA. Cell Death Differ 26: 2329-2343, 2019.
48. Gai C, Yu M, Li Z, Wang Y, Ding D, Zheng J, Lv S, Zhang W and Li W: Acetaminophen sensitizing erastin-induced ferroptosis via modulation of Nrf2/heme oxygenase-1 signaling pathway in non-small-cell lung cancer. J Cell Physiol 235: 3329-3339, 2020.
49. Cui Z, Fu Y, Yang Z, Gao Z, Feng H, Zhou M, Zhang L and Chen C: Comprehensive analysis of a ferroptosis pattern and associated prognostic signature in acute myeloid leukemia. Front Pharmacol 13: 866325, 2022.
50. Wang Y, Yang J, Chen S, Wang W and Teng L: Identification and validation of a prognostic signature for thyroid cancer based on ferroptosis-related genes. Genes (Basel) 13: 997, 2022.
51. Fan R, Chen Y, Nechuta S, Cai H, Gu K, Shi L, Bao P, Shyr Y, Shu XO and Ye F: Prediction models for breast cancer prognosis among Asian women. Cancer 127: 1758-1769, 2021.
52. Yang YF, Lee YC, Wang YY, Wang CH, Hou MF and Yuan SF: YWHAE promotes proliferation, metastasis, and chemoresistance in breast cancer cells. Kaohsiung J Med Sci 35: 408-416, 2019.
53. Liu T, Jiang L, Tavana O and Gu W: The Deubiquitylase OTUB1 mediates ferroptosis via stabilization of SLC7A11. Cancer Res 79: 1913-1924, 2019.
54. Zou Y, Palte MJ, Deik AA, Li H, Eaton JK, Wang W, Tseng YY, Deasy R, Kost-Alimova M, Dančík V, *et al*: A GPX4-dependent cancer cell state underlies the clear-cell morphology and confers sensitivity to ferroptosis. Nat Commun 10: 1617, 2019.
55. Lang X, Green MD, Wang W, Yu J, Choi JE, Jiang L, Liao P, Zhou J, Zhang Q, Dow A, *et al*: Radiotherapy and immunotherapy promote tumoral lipid oxidation and ferroptosis via synergistic repression of SLC7A11. Cancer Discov 9: 1673-1685, 2019.
56. Lee YH, Kim HS, Kim JS, Yu MK, Cho SD, Jeon JG and Yi HK: C-myb regulates autophagy for pulp vitality in glucose oxidative stress. J Dent Res 95: 430-438, 2016.
57. Minekura H, Kang MJ, Inagaki Y, Suzuki H, Sato H, Fujino T and Yamamoto TT: Genomic organization and transcription units of the human acyl-CoA synthetase 3 gene. Gene 278: 185-192, 2001.
58. Hao S, Yu J, He W, Huang Q, Zhao Y, Liang B, Zhang S, Wen Z, Dong S, Rao J, *et al*: Cysteine dioxygenase 1 mediates erastin-induced ferroptosis in human gastric cancer cells. Neoplasia 19: 1022-1032, 2017.
59. Alfarsi LH, El Ansari R, Masisi BK, Parks R, Mohammed OJ, Ellis IO, Rakha EA and Green AR: Integrated analysis of key differentially expressed genes identifies DBN1 as a predictive marker of response to endocrine therapy in luminal breast cancer. Cancers (Basel) 12: 1549, 2020.
60. Wang X, Fu Y, Chen X, Ye J, Lü B, Ye F, Lü W and Xie X: The expressions of bHLH gene HES1 and HES5 in advanced ovarian serous adenocarcinomas and their prognostic significance: A retrospective clinical study. J Cancer Res Clin Oncol 136: 989-996, 2010.
61. Konishi J, Kawaguchi KS, Vo H, Haruki N, Gonzalez A, Carbone DP and Dang TP: Gamma-secretase inhibitor prevents Notch3 activation and reduces proliferation in human lung cancers. Cancer Res 67: 8051-8057, 2007.
62. Li X, Cao Y, Li M and Jin F: Upregulation of HES1 promotes cell proliferation and invasion in breast cancer as a prognosis marker and therapy target via the AKT pathway and emt process. J Cancer 9: 757-766, 2018.
63. Li X, Li Y, Du X, Wang X, Guan S, Cao Y, Jin F and Li F: HES1 promotes breast cancer stem cells by elevating slug in triple-negative breast cancer. Int J Biol Sci 17: 247-258, 2021.
64. Sun X, Ou Z, Xie M, Kang R, Fan Y, Niu X, Wang H, Cao L and Tang D: HSPB1 as a novel regulator of ferroptotic cancer cell death. Oncogene 34: 5617-5625, 2015.
65. Jiang XP, Elliott RL and Head JF: Manipulation of iron transporter genes results in the suppression of human and mouse mammary adenocarcinomas. Anticancer Res 30: 759-765, 2010.
66. Emens LA: Breast cancer immunotherapy: Facts and hopes. Clin Cancer Res 24: 511-520, 2018.
67. Dunn GP, Bruce AT, Ikeda H, Old LJ and Schreiber RD: Cancer immunoediting: From immunosurveillance to tumor escape. Nat Immunol 3: 991-998, 2002.
68. Jia M, Qin D, Zhao C, Chai L, Yu Z, Wang W, Tong L, Lv L, Wang Y, Rehwinkel J, *et al*: Redox homeostasis maintained by GPX4 facilitates STING activation. Nat Immunol 21: 727-735, 2020.
69. Maldonado EN and Lemasters JJ: Warburg revisited: Regulation of mitochondrial metabolism by voltage-dependent anion channels in cancer cells. J Pharmacol Exp Ther 342: 637-641, 2012.
70. Yagoda N, von Rechenberg M, Zaganjor E, Bauer AJ, Yang WS, Fridman DJ, Wolpaw AJ, Smukste I, Peltier JM, Boniface JJ, *et al*: RAS-RAF-MEK-dependent oxidative cell death involving voltage-dependent anion channels. Nature 447: 864-868, 2007.
71. Ponde NF, Zardavas D and Piccart M: Progress in adjuvant systemic therapy for breast cancer. Nat Rev Clin Oncol 16: 27-44, 2019.